



# A 3-D semi-coupled numerical model for fluid–structures–seabed-interaction (FSSI-CAS 3D): Model and verification

Jianhong Ye<sup>a,b,\*</sup>, Dongsheng Jeng<sup>b,c</sup>, Ren Wang<sup>a</sup>, Changqi Zhu<sup>a</sup>

<sup>a</sup> State Key Laboratory of Geomechanics and Geotechnical Engineering, Institute of Rock and Soil Mechanics, Chinese Academy of Sciences, Wuhan 430071, China

<sup>b</sup> Division of Civil Engineering, University of Dundee, Dundee DD1 4HN, UK

<sup>c</sup> Center for Marine Geotechnical Engineering, Shanghai Jiao Tong University, Shanghai 200240, China

## ARTICLE INFO

### Article history:

Received 7 February 2012

Accepted 30 March 2013

Available online 17 May 2013

### Keywords:

Fluid–structures–seabed-interaction

Biot's equation

Modified Navier–Stokes equation

Coupled numerical model

Porous seabed

Breakwater

Nonlinear drag force

## ABSTRACT

In this study, a semi-coupled 3-D numerical model for fluid–structures–seabed-interaction is developed. The dynamic Biot's equation known as “ $u$ – $p$ ” approximation, and modified Navier–Stokes equation in which the linear drag force between the flowing pore water and the solid matrix of porous medium is included, is respectively adopted as the governing equation in the soil sub-model and the wave sub-model. A coupling algorithm is developed to integrate the two sub-models together, in which non-match mesh and non-match time scheme are used based on the shepherd interpolation method. The data exchange is implemented at the interface between fluid domain and seabed/marine structures domain adopting the coupling algorithm. Finally, the developed 3-D numerical model is validated by an analytical solution and a laboratory wave flume test.

© 2013 Elsevier Ltd. All rights reserved.

## 1. Introduction

In recent two decades, more and more marine structures, such as breakwater, oil platform and turbine, have been constructed in offshore areas. The response of seabed foundation, and the stability of marine structures built on seabed foundation under ocean wave loading becomes the main issue most concerned by coastal engineers involved in design of marine structures. In coastal zones, the breakwaters are widely used to protect the coastline from damage and erosion, and also could protect the people living in the zones near the coastline from death and properties loss induced by the probable tsunami attack. However, the breakwaters built on porous seabed are vulnerable to the liquefaction and the shear failure of seabed foundation (Chung et al., 2006; Franco, 1994; Lundgren et al., 1989). In the practice of engineering, an inappropriate design and maintenance of a breakwater would result in the collapse of breakwater after construction, and further bring great economic loss. Therefore, it is meaningful to develop an effective analysis tool for coastal engineers to predict and evaluate the stability (liquefaction and shear failure) of seabed foundation beneath the marine structures under wave loading.

Some investigations have been conducted on the problem of fluid–breakwater–seabed interaction (FSSI) in the last 20 years. These investigations included analytical solutions (Hsu et al., 1993; Tsai, 1995; Tsai et al., 2000), decoupled numerical model (Mase et al., 1994; Ulker et al., 2010, 2012) and coupled numerical model (Cheng et al., 2007; Hur and

\* Corresponding author at: State Key Laboratory of Geomechanics and Geotechnical Engineering, Institute of Rock and Soil Mechanics, Chinese Academy of Sciences, Wuhan 430071, China. Tel.: +86 27 87197591.

E-mail address: yejianhongcas@gmail.com (J.H. Ye).

Mizutani, 2003; Hur et al., 2008, 2010; Mizutani and Mostafa, 1998; Mizutani et al., 1998, 1999; Mostafa et al., 1999). Among these proposed analytical solutions for the FSSI problem, only the cases in which simple boundary conditions were involved could be dealt with; for example, the Stokes waves were used to apply the wave-induced pressure on seabed; and the breakwater was simplified as a line without width and weight; the wave-induced pressure on breakwater could not be taken into consideration. The application of decoupled numerical models to the FSSI problem also deserved some inevitable constraints. The linear or nonlinear Stokes waves were adopted to apply the wave-induced pressure acting seabed and breakwater in numerical computation. Hence, the effect of the outer shape of breakwater and the porosity of seabed and rubble mound on the wave characteristics near the breakwater was ignored. For example, the linear standing wave was used to apply the loading on seabed and breakwater in Mase et al. (1994) and Ulker et al. (2010, 2012). Actually, the wave field in front of the breakwater was not a standing wave due to the fact that the front lateral side of breakwater was not a vertical wall.

The coupled numerical model is an ideal method for the FSSI problem. At present, there are two types of coupled numerical models available for the FSSI problem in literatures. The first type coupled model emphasizes its attention on the interaction between the seawater and the pore water in seabed and porous marine structures, such as rubble mound breakwater (Hur and Mizutani, 2003; Hur et al., 2008, 2010). The effect of the outer shape of breakwater and the porosity of seabed and rubble mound on the wave characteristics near the breakwater could be sufficiently considered. However, the wave induced effective stress status in seabed and breakwater could not be determined. The second type coupled model further integrates the governing equation of fluid into Biot's equation to study the FSSI problem. The wave induced effective stress status in seabed and breakwater can be determined (Cheng et al., 2007; Mizutani and Mostafa, 1998; Mizutani et al., 1998, 1999; Mostafa et al., 1999, ). Due to the fact that the Navier–Stokes equation, and  $k-\epsilon$  turbulence model are used for the wave motion in seawater, the interaction between a complex wave (such as breaking wave), seabed and breakwater is possible to be simulated. For example, most recently, adopting the 2-D coupled model developed by Ye (2012) and Ye et al. (submitted for publication) investigates the interaction between a breaking wave, porous coastal slopes and a composite breakwater, and studies the wave-induced momentary liquefaction in the seabed foundation in front of the composite breakwater. Detailed review for the wave–seabed–breakwater interaction can be found in Ye (2012).

To the author's knowledge, all previous coupled numerical models are limited to two dimensional cases. There is no 3-D coupled numerical model to investigate the FSSI problem. In this study, a 3-D coupled numerical model is developed for the 3-D FSSI problem, in which two sub-models are included: soil model and wave model. Biot's dynamic equation is used as the governing equation in the soil model; the modified Navier–Stokes equation, in which the linear drag force between the flowing pore water and the solid matrix of porous medium is included, is used to govern the wave motion in the wave model. A coupling algorithm is developed to integrate the two sub-models together. Finally, the developed model is validated by an analytical solution and a laboratory wave flume test. Actually, this 3-D numerical model is a continuation of the previous 2-D numerical model for FSSI problem developed by Ye et al. (submitted for publication, in press).

## 2. Semi-coupled 3-D numerical model

### 2.1. Soil model

It is well known that the seabed is a porous medium consisting of the soil particles, pore water and trapped air. Biot's theory is widely adopted to describe the mechanical behaviors of porous medium. In this numerical model, the dynamic Biot's equation known as “ $u-p$ ” approximation proposed by Zienkiewicz et al. (1980) is used as the governing equation for 3-D porous seabed. The relative displacements of pore water to the soil particles are ignored; however, the acceleration of the pore water and soil particles are considered in the governing equation.

The equilibrium equations are

$$\frac{\partial \sigma'_x}{\partial x} + \frac{\partial \tau_{xy}}{\partial y} + \frac{\partial \tau_{xz}}{\partial z} = -\frac{\partial p_s}{\partial x} + \rho \frac{\partial^2 u_s}{\partial t^2}, \tag{1}$$

$$\frac{\partial \tau_{xy}}{\partial x} + \frac{\partial \sigma'_y}{\partial y} + \frac{\partial \tau_{yz}}{\partial z} = -\frac{\partial p_s}{\partial y} + \rho \frac{\partial^2 v_s}{\partial t^2}, \tag{2}$$

$$\frac{\partial \tau_{xz}}{\partial x} + \frac{\partial \tau_{yz}}{\partial y} + \frac{\partial \sigma'_z}{\partial z} + \rho g = -\frac{\partial p_s}{\partial z} + \rho \frac{\partial^2 w_s}{\partial t^2}. \tag{3}$$

The mass continuity of pore water is

$$k\nabla^2 p - \gamma_w n \beta \frac{\partial p_s}{\partial t} + k \rho_f \frac{\partial^2 \epsilon_v}{\partial t^2} = \gamma_w \frac{\partial \epsilon_v}{\partial t}, \tag{4}$$

where  $u_s$ ,  $v_s$ , and  $w_s$  are the soil displacements in the  $x$ ,  $y$ , and  $z$  directions, respectively;  $n$  is the porosity of soil;  $\sigma'_x$ ,  $\sigma'_y$  and  $\sigma'_z$  are the effective normal stresses in the horizontal and vertical directions;  $\tau_{xy}$ ,  $\tau_{yz}$  and  $\tau_{xz}$  are the shear stresses;  $p_s$  is the pore pressure in porous medium;  $\rho = n\rho_f + (1-n)\rho_s$  is the average density of porous medium;  $\rho_f$  is the fluid density;  $\rho_s$  is the solid density;  $k$  is Darcy's permeability;  $g$  is the gravitational acceleration and  $\gamma_w$  is the unit water weight.  $\epsilon_v$  is the

volumetric strain. In Eq. (4), the compressibility of pore fluid ( $\beta$ ) and the volume strain ( $\epsilon_v$ ) are defined as

$$\epsilon_v = \frac{\partial u_s}{\partial x} + \frac{\partial v_s}{\partial y} + \frac{\partial w_s}{\partial z}, \quad (5)$$

$$\beta = \frac{1}{K_f} + \frac{1-S_r}{p_{w0}}, \quad (6)$$

where  $S_r$  is the degree of saturation of seabed, defined as the ratio of the volume of pore water to the volume of soil ( $S_r = V_w/V$ );  $p_{w0}$  is the absolute static pressure and  $K_f$  is the bulk modulus of pore water; generally,  $K_f = 2.24 \times 10^9$  N/m<sup>2</sup> for pore water.

If the seabed has anisotropic permeability,  $k$  could be expressed as

$$k = k_{ij} = \begin{bmatrix} k_x & 0 & 0 \\ 0 & k_y & 0 \\ 0 & 0 & k_z \end{bmatrix}. \quad (7)$$

For isotropic porous seabed, the permeability coefficients should be the same in three directions:  $k_x = k_y = k_z$ .

The finite element method is used to solve the above governing Eqs. (1)–(4). The Generalized Newmark- $\beta$  method is adopted for the time integration for dynamic problem. Chan (1988) developed a 2-D FEM program SWANDYNE solving the “ $u-p$ ” approximation to specially investigate the seismic wave-induced response of porous sand bed. The wave loading on seabed and marine structures could not be applied in this program. Recently, Ye (2012) and Ye et al. (in press) further developed the above 2-D FEM code to investigate the wave-seabed-breakwater interaction. Ou (2009) further extended the above 2-D FEM code SWANDYNE to 3-D. However, only simple loading could be applied in this 3-D code. Based on Ou (2009)’s work, Ye (2012) developed a new loading system to replace the old one in the 3-D FEM code. The new loading system developed can deal with various boundary conditions, such as time-dependent forces, pressure and displacement, on arbitrary planes at arbitrary directions in 3-D space. The finite element formulations of soil model can be found in Ye (2012). In this 3-D FEM program, it is noted that the compressive stress is taken as negative value, and the displacement toward the direction of axes is taken as positive value.

In this study, the seabed foundation is treated as a poro-elastic medium. The linear poro-elastic constitutive model is used to describe the mechanical behavior of porous seabed foundation under ocean wave loading. The elastic matrix  $D$  under the condition of plane strain is expressed as

$$D = \frac{E}{(1+\nu)(1-2\nu)} \begin{bmatrix} 1-\nu & \nu & 0 \\ \nu & 1-\nu & 0 \\ 0 & 0 & \frac{1-2\nu}{2} \end{bmatrix},$$

where  $E$  and  $\nu$  are the elastic modulus and Poisson’s ratio of soil, respectively. One of the inadequacies of the linear poro-elastic model is that the nonlinear deformation behavior of soil cannot be described in computation. In nature, only the dense soils with high value of relative density  $D_r$  could show the elastic deformation under low level loading. There is basically no dilation and compaction of soil in the process of loading. For the newly deposited offshore soil, or the dense soil under high level loading, the dilation or compaction of soil will occur in the process of loading. The plastic deformation of soil is the dominant part. Under such a situation, the poro-elastoplastic models should be used. The elastoplastic matrix  $D^{ep}$  under the condition of plane strain can be expressed as in the form of tensor:

$$D_{ijkl}^{ep} = D_{ijkl}^e - \frac{D_{ijmn}^e m_{mn} n_{st} D_{stkl}^e}{H_{L/U} + n_{st} D_{stkl}^e m_{kl}},$$

in which  $D_{ijkl}^e$  is the tensor form of elastic matrix  $D$ .  $H_{L/U}$  is the plastic modulus at loading or unloading stage.  $m_{mn}$  is the plastic flow direction tensor, and  $n_{st}$  is the loading or unloading direction tensor. The interaction between wave, marine structures and poro-elastoplastic seabed has been conducted by Ye (2012), and will be published later.

## 2.2. Wave model

The wave motion on seabed, and the interaction with marine structures are governed by using a modified Navier–Stokes equation, in which the porous flow in porous marine structures can be considered. The seawater is treated as incompressible Newtonian fluid:

$$\nabla u_{fi} = 0, \quad (8)$$

$$\rho_f \left( \frac{\partial u_{fi}}{\partial t} + u_{fj} \cdot \nabla u_{fi} \right) = -\nabla p + \nabla \cdot \tau + g_i + f_{S_i} + f_{D_i}, \quad (9)$$

where  $u_{fi}$  ( $i=x, y, z$ ) represents the velocities of seawater,  $\rho_f$  is the water density,  $p$  is the water pressure,  $g$  is the gravity, and  $f_S$  is the surface tension forces.  $\tau = \mu(\nabla u_{fi} + \nabla^T u_{fi})$  is the shear stress tensor,  $\mu$  is the dynamic viscosity of seawater, and  $f_D$  is the drag force used to describe the porous flow in the presence of a porous medium. Here, Darcy’s law is used to describe the interaction between the pore water and the solid matrixes of porous medium. It assumes that the drag force is linearly

dependent on the fluid superficial velocity. The drag force is formulated as (Hur et al., 2010)

$$f_{Di} = C_D \frac{\mu}{d_{50}^2} \frac{(1-n)^2}{n} u_{fi}, \tag{10}$$

in which  $C_D$  is the laminar porous flow induced drag force coefficient, and it is mainly related to the particles' shapes of solid matrix. In Eq. (10), the effect of the average diameter of particles in solid matrix on the drag force is considered.

In this coupled numerical model, the above governing Eqs. (8) and (9) for the wave motion and the porous flow in porous marine structures are solved by using the free platform provided by the open source code TRUCHAS (2009) developed by the US Los Alamos National Laboratory (LANL) (2009). In TRUCHAS, the finite volume method is adopted to solve the governing equations, and the VOF method is adopted to trace the free surface of wave motion. The detailed physical algorithms can be found in the manual (TRUCHAS, 2009). In the original source code of TRUCHAS, the Carman–Koseny relation proposed by Carman (1937) is adopted to formulate the linear drag force:

$$f_{Di} = k_{ij} \frac{(1-n)^2}{n^3} u_{fi}, \tag{11}$$

in which  $k_{ij}$  and  $n$  are the permeability and porosity of porous medium respectively. Obviously, the viscosity of fluid, the average particles diameter, and the effect of particles shape are all not taken into consideration. The porous flow module in the original source code of TRUCHAS has been modified to adopt Eq. (10) to describe the linear drag force.

In this wave model, the internal wave maker proposed by Lin and Liu (1999) is applied to generate the target wave train, in which a mass function is added to the continuity equation (8) at the position where the wave maker is located. By applying different mass functions, various waves could be generated, for example, the linear wave, solitary wave, 2nd-order and 5th-order Stokes wave, cnoidal wave etc.

### 2.3. Coupling algorithm

In the coupling process, the data exchange between the two models is an important issue that needs to be solved. As we know, generally, the mesh size used in fluid domain is relatively small, while, the mesh size used in solid domain is relatively huge. The ratio between the mesh size used in solid domain and fluid domain would be 10–20. Therefore, it is not wise to share the computational nodes on the interface between the fluid domain and solid domain. Otherwise, the number of meshes in solid domain in coupling computation would increase greatly; however, it is not meaningful to improve the computational accuracy. In this study, the non-match mesh scheme is used in the coupling computation (Fig. 1). A data

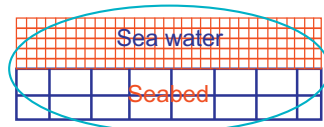


Fig. 1. Non-match mesh scheme is used in the coupling of seawater and seabed.

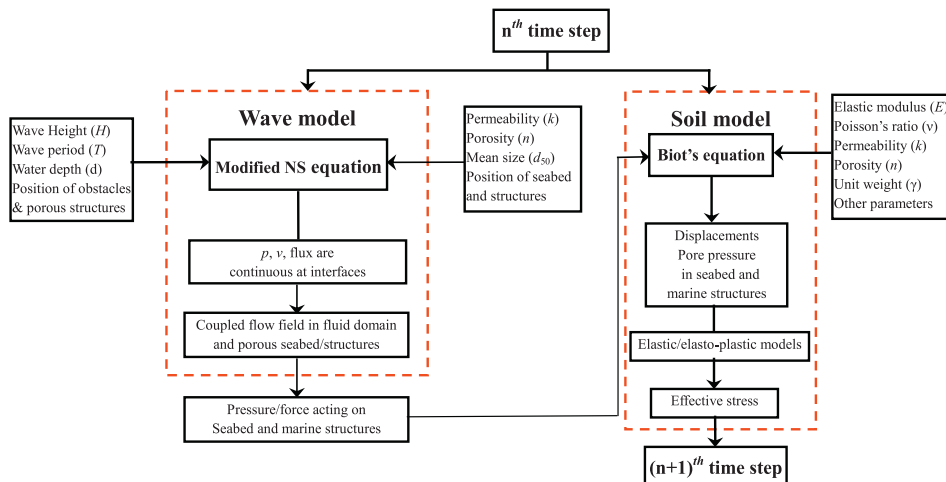


Fig. 2. Coupling algorithms between the modified Navier–Stokes equation and Biot's equation (after Ye, 2012).

exchange port is developed adopting the 3-D Shepard interpolation method to transmit data at the interface between the fluid domain and solid domain.

In the coupled model, the wave model is governed by the modified Navier–Stokes equations, and the soil model is governed by the dynamic Biot's equations. In the wave model, the continuity of pressure, velocity/flux of fluid at the interface between seawater and porous seabed/marine structures is considered. Therefore, the flow field in fluid domain and in porous seabed/marine structures is fully coupled. When coupling the Navier–Stokes equations and dynamic Biot's equations, only the pressure continuity on the interfaces is applied in calculation; however, the continuity of displacements on the interfaces between the fluid domain and solid domain is not applied. That is the reason why we call this coupled numerical model as a 'semi-coupled' model. In the practice of offshore engineering, generally the magnitude of wave-induced vibration of marine structures is apparently minor compared to the wave length. The discontinuity of displacement on the interfaces is completely acceptable from the point of view of engineering practice. In the coupling computation, the wave model is responsible for the generation, propagation of wave, and the porous flow in porous structures, such as seabed, rubble mound breakwater etc., and determines the pressure acting on the seabed and marine structures. In the meantime, the pressure/force acting on seabed and marine structures determined by the wave model is provided to the soil model through the data exchange port developed to calculate the dynamic response of seabed and marine structures, including the displacements, pore pressure and the effective stresses. The coupling process is illustrated in Fig. 2.

### 3. Verification of coupled model

#### 3.1. Analytical verification

The analytical solution of dynamic response of a seabed (without marine structure) under linear progressive wave loading proposed by Hsu and Jeng (1994) is used to verify the 3-D coupled model in this part. In coupling computation,

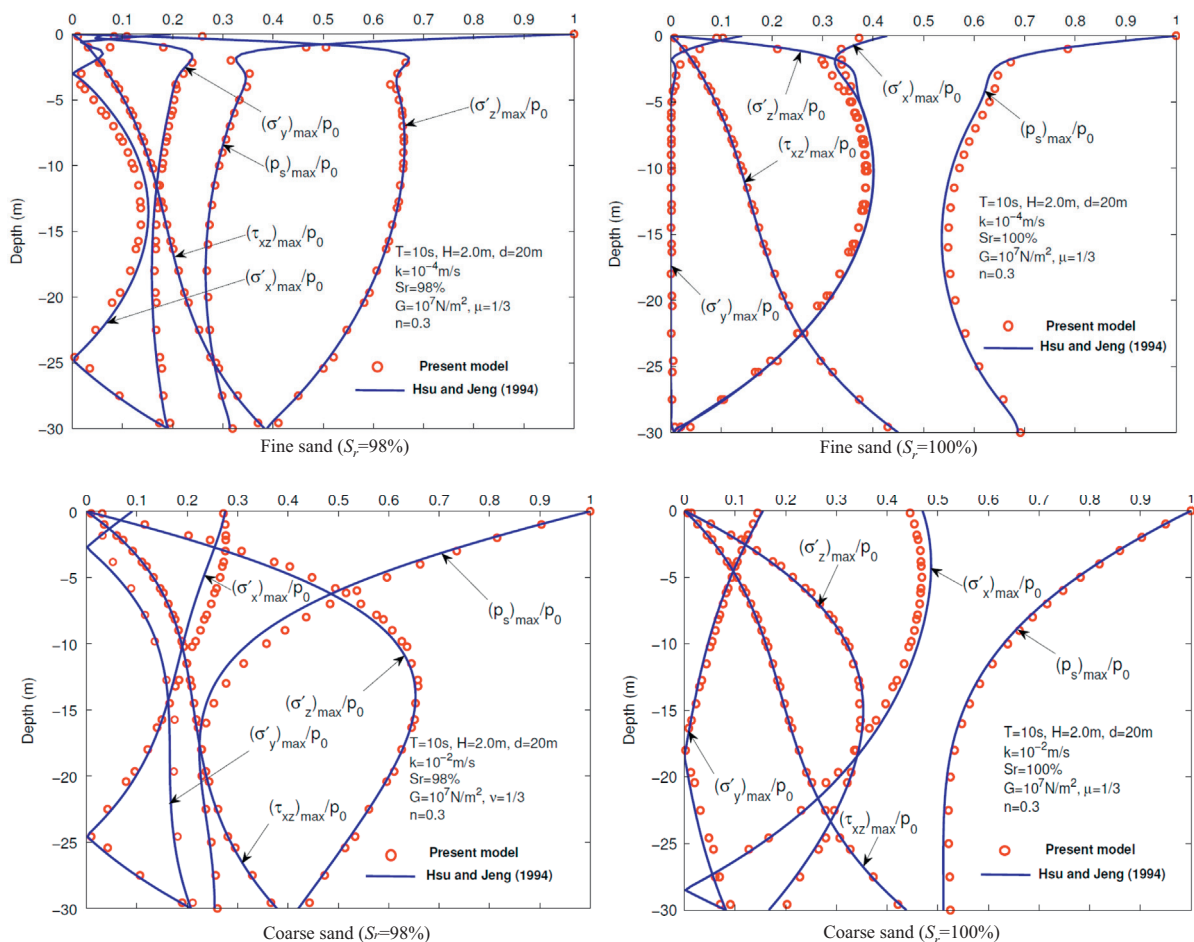


**Fig. 3.** Comparison of the linear wave-induced seabed response between the numerical results determined by developed coupled model and the analytical solution (after Ye, 2012). Fine sand ( $S_r=98\%$ ), fine sand ( $S_r=100\%$ ), coarse sand ( $S_r=98\%$ ), coarse sand ( $S_r=100\%$ ).

the progressive wave propagating on a flat seabed floor is determined by the 3-D wave model according to the given water wave parameters. The wave induced wave pressure acting on seabed is transmitted to the soil model through the developed data exchange port. The dynamic response of seabed under the wave loading is then determined by the 3-D FEM soil model. The length of computational domain is one wave length, and the periodical boundary condition is applied to the two lateral boundaries along the wave propagating direction. The thickness and width of model are both 30 m. The comparisons between the numerical and analytical results are illustrated in Fig. 3. As shown in Fig. 3, the numerical results determined by the present coupled numerical model agree very well with the analytical solution. It is indicated that the 3-D numerical model is applicable to the problem of 3-D wave–seabed interaction. Figs. 4 and 5 show the wave induced pore pressure, effective stresses and displacements in a coarse sand bed ( $S_r=98\%$ ) under the linear wave loading at a time. At this moment, the wave trough is passing the middle part of the coarse sand bed.

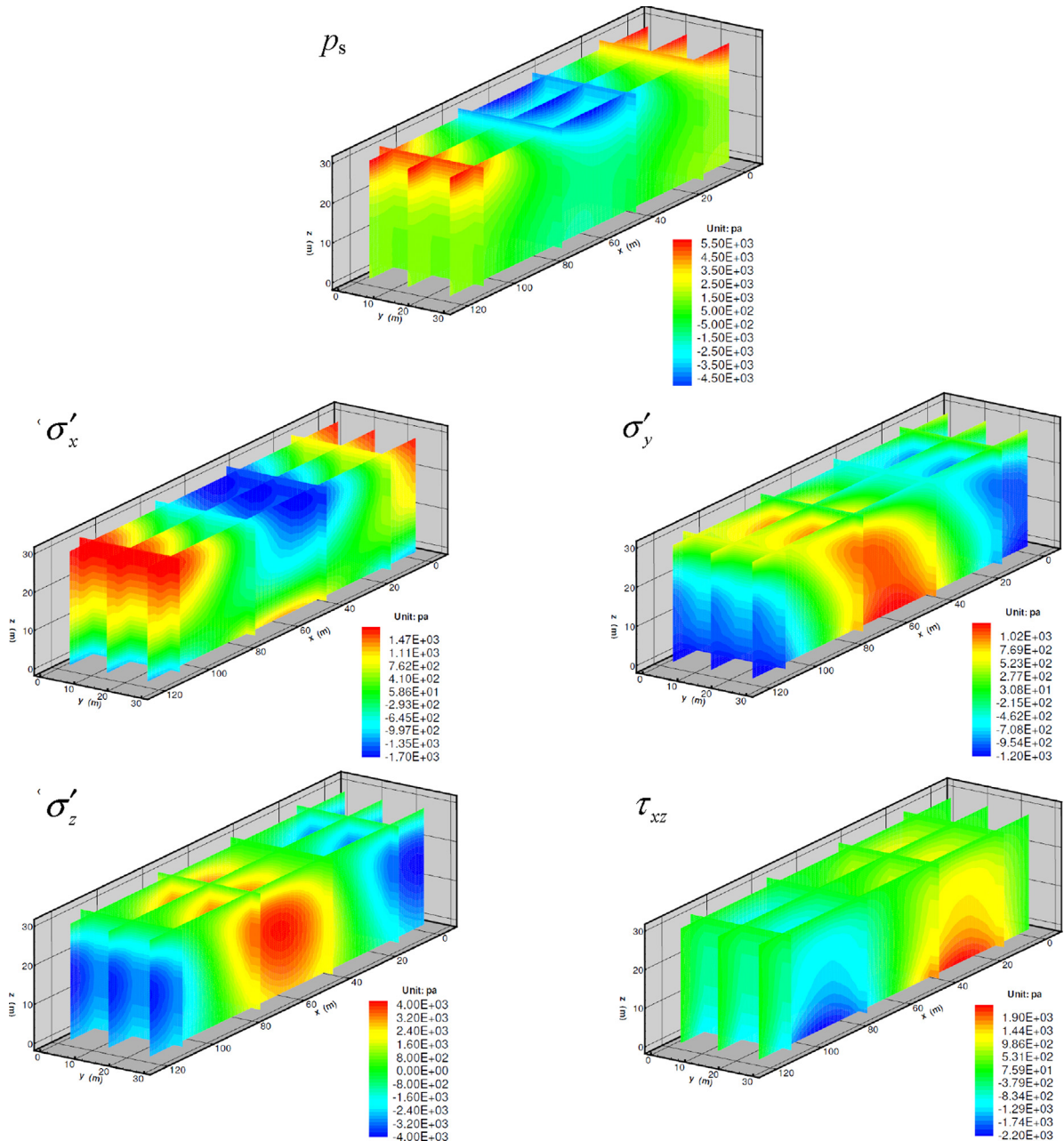


Fig. 4. Distribution of wave-induced pore pressure and effective stress in 3-D coarse sand seabed ( $S_r=98\%$ ) at a time.

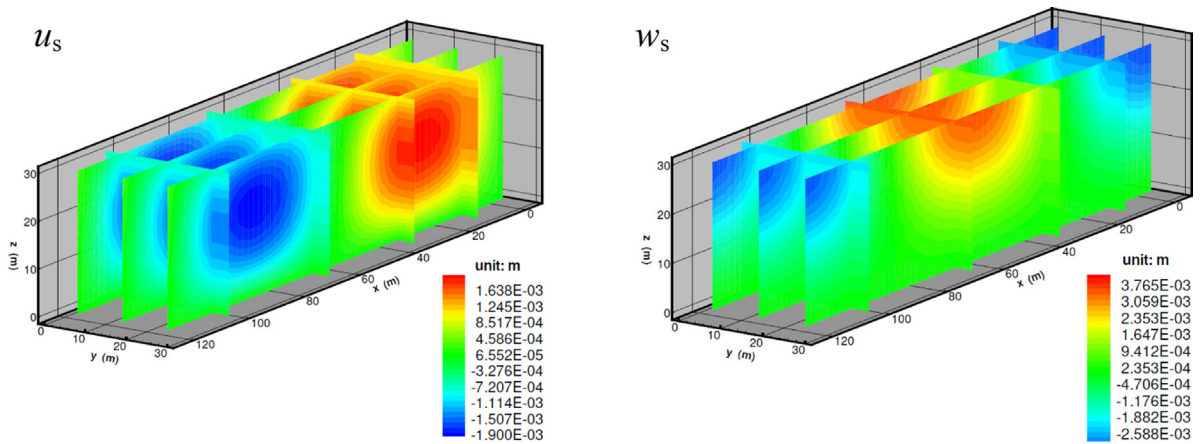


Fig. 5. Distribution of wave-induced displacements  $u_s$  and  $w_s$  in 3-D coarse sand seabed ( $S_r=98\%$ ) at a time.

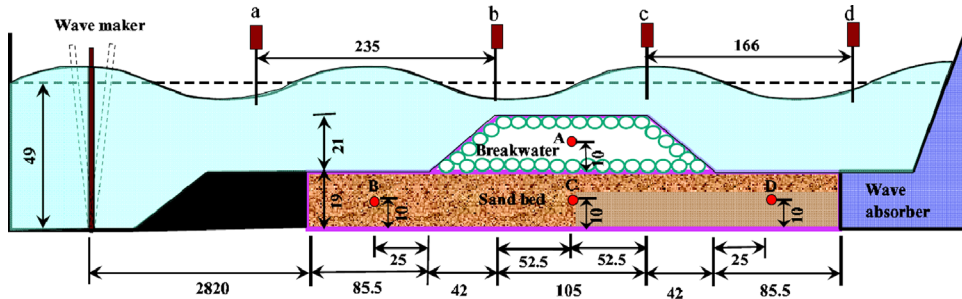


Fig. 6. Experimental setup in the wave flume test conducted by Mizutani et al. (1998).

Table 1  
Properties of the sand bed and rubble mound breakwater.

	$G$ (MPa)	$\nu$	$K$ (cm/s)	$n$	$d_{50}$ (mm)	$S_r$ (%)
Sand bed	500	0.33	0.22	0.3	1.0	99
Breakwater	1000	0.24	18	0.33	30	99

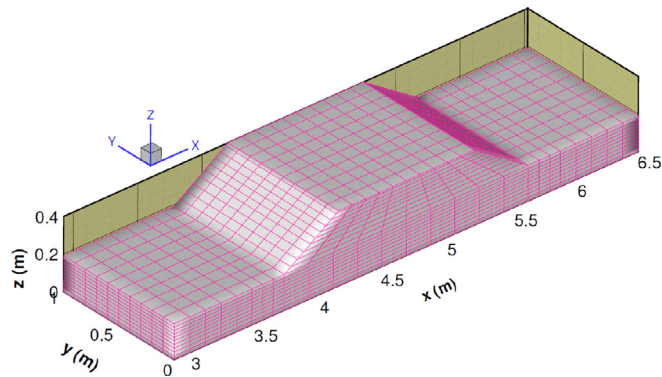


Fig. 7. 27-nodes isoparametric brick element is used for the rubble mound breakwater and seabed.

### 3.2. Experimental verification

In this section, the above developed 3-D coupled numerical model is validated by using a wave flume test conducted by Mizutani et al. (1998). Mizutani et al. (1998) conducted a wave flume test to investigate the interaction between the regular

wave, submerged breakwater and sand bed. The experiment setup is shown in Fig. 6 (noted: the width is 1.0 m in y direction). In the experiment, a submerged rubble mound breakwater is constructed on a sand bed. Four wave height meters are installed at points *a*, *b*, *c* and *d* to monitor the wave profile. Four pore pressure sensors are installed at points A, B, C and D to record the wave induced pore pressure. The properties of the sand bed and rubble mound breakwater provided by Mizutani et al. (1998) are listed in Table 1. Due to the fact that the wave steepness is only  $0.03/2.1 = 0.014286$ , the second-order wave maker model is enough to accurately simulate the generation, propagation of the wave in the wave flume.

### 3.2.1. Consolidation

In the experimental test, the test tank is firstly filled with sandy soil, and the breakwater is built on the sandy bed. Then, the wave flume is filled with water to the specified depth. The sandy bed consolidates under the breakwater and hydrostatic water pressure for several days. This consolidation process of sandy bed under the rubble mound breakwater and hydrostatic water pressure should be first determined. FSSI-CAS 3D can simulate this consolidation process through setting the wave height as zero. The 27-nodes isoparametric brick element is used to discretize the rubble mound breakwater in computation (Fig. 7).

Fig. 8 shows the distribution of pore pressure and effective stresses in the sand bed and breakwater when the consolidation process is finished. From Fig. 8, it can be seen that there is no excess pore pressure in the sand bed and breakwater, and the pore pressure is layered. The construction of breakwater on the sand bed makes the effective stresses increase significantly in the zone under the breakwater. There is a very thin layer in which tensile  $\sigma'_x$  exists at the bottom

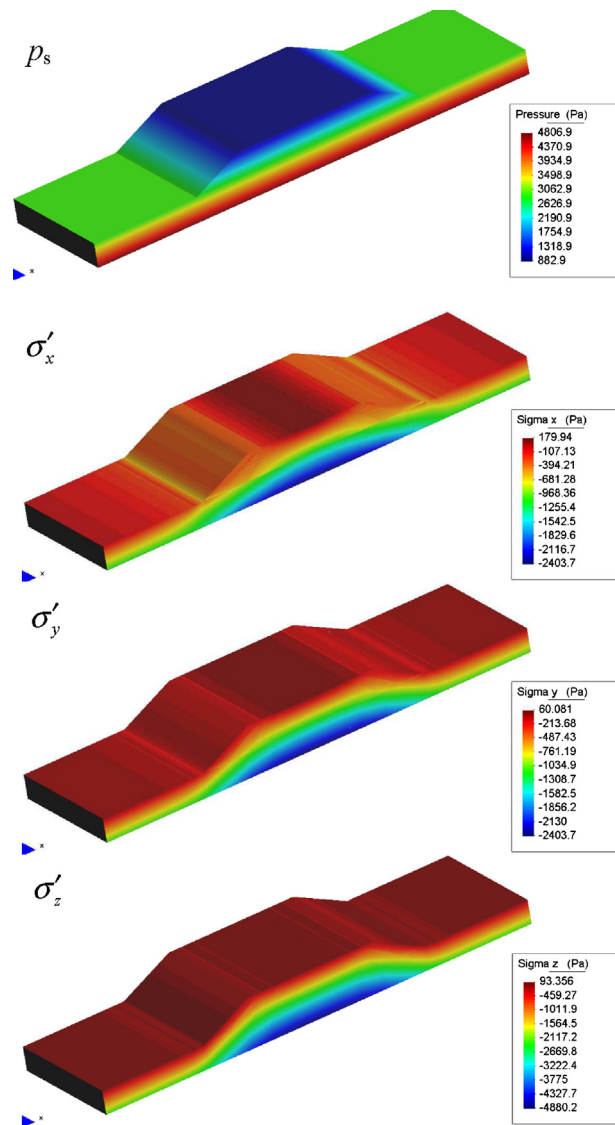


Fig. 8. Distribution of pore pressure and effective stresses at the final consolidation status.

zone of rubble mold breakwater. This would be attributed to the fact that the sandy bed is much softer than the breakwater. It results in the deformation of breakwater and sandy bed is inconsistent.

Fig. 9 shows the distribution of horizontal and vertical displacement  $u_s$  and  $w_s$  at the final consolidation status in the sand bed and rubble mound breakwater. From these two distributions of displacement, it is found that the sand bed moves toward the two lateral sides under the compression of overburdened breakwater. The horizontal displacement mainly occurs in the zone under the two feet of breakwater. Another phenomenon observed from Fig. 9 is that the breakwater subsides downward in the consolidation process, and the settlement is not uniform. The maximum settlement occurs at the middle part of breakwater.

### 3.2.2. 3-D wave field

Taking the above final consolidated status of sandy bed under breakwater and hydrostatic pressure as the initial condition, the coupled numerical model FSSI-CAS 3D is continuously adopted to simulate the interaction between the wave, submerged breakwater and sandy bed. In coupling computation, the sand bed and rubble mound breakwater are treated as different porous structures in fluid domain in the wave model. The data exchange is implemented by the coupling algorithm at the interface between the solid domain (sand bed, breakwater) and the fluid domain. In the soil model, the sand bed and the breakwater are also treated as different porous mediums with different properties listed in Table 1. The wave characteristics in Mizutani et al. (1998)'s experiment are wave height  $H=0.03$  m, water depth  $d=0.3$  m, and wave period  $T=1.4$  s. The wave maker is placed at the position  $x=-2$  m to generate the expected wave train propagating in wave flume. Two sponge layers placed at  $x=-6-4$  m (left end of wave flume), and  $x=9-11$  m (right end of wave flume) are set to absorb the wave energy, to prevent the appearance of reflected wave.

Fig. 10 illustrates the 3-D wave profile at several typical times determined by the FSSI-CAS 3D in the process of wave, sand bed and breakwater interaction. From Fig. 10, it can be seen that the water on sand bed is static at the beginning of computation. At time  $t=3.36$  s, the wave does not arrive at the breakwater. At time  $t=6.58$  s, the first wave crest is passing through the breakwater. After that, a series of wave crests and wave troughs pass through the breakwater. In Fig. 10, it is observed that the wave profile in the zone behind the breakwater is completely different from that in the zone in front of breakwater. The wave length becomes much shorter in the zone behind the breakwater. It is indicated that the rubble mound breakwater could effectively block the wave propagation, and dissipate the wave energy. The sand bed behind the breakwater could be effectively protected by the breakwater.

Fig. 11 demonstrates the comparison of the wave profile at the four typical positions  $a$ ,  $b$ ,  $c$  and  $d$  between the experimental data (Mizutani et al., 1998) and the numerical results determined by FSSI-CAS 3D. As demonstrated in Fig. 11, the agreement for the wave profile at the positions in front of the breakwater is very good. However, the agreement at the position behind the breakwater is not very good, but is acceptable. The difference is most significant at position  $d$ . There is obviously a phase difference between the experimental wave profile and the numerical results. This phase difference would attribute to the usage of a simple formulation (Eq. (10)) to describe the drag force between the porous flow and the solid matrixes in the breakwater. The average diameter  $d_{50}$  of the rubble mound breakwater is 3 cm, which is 30 times that of the sand bed. The recent investigations (Hur et al., 2008, 2010) point out that the porous flow in porous medium with huge

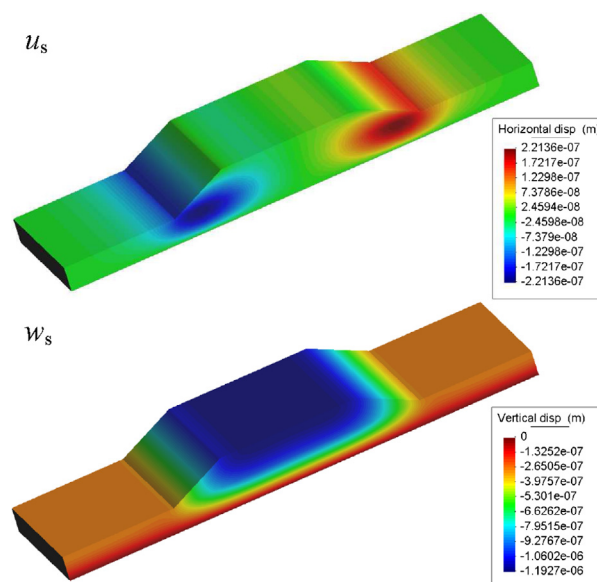


Fig. 9. Distribution of horizontal and vertical displacement  $u_s$  and  $w_s$  at the final consolidation status.

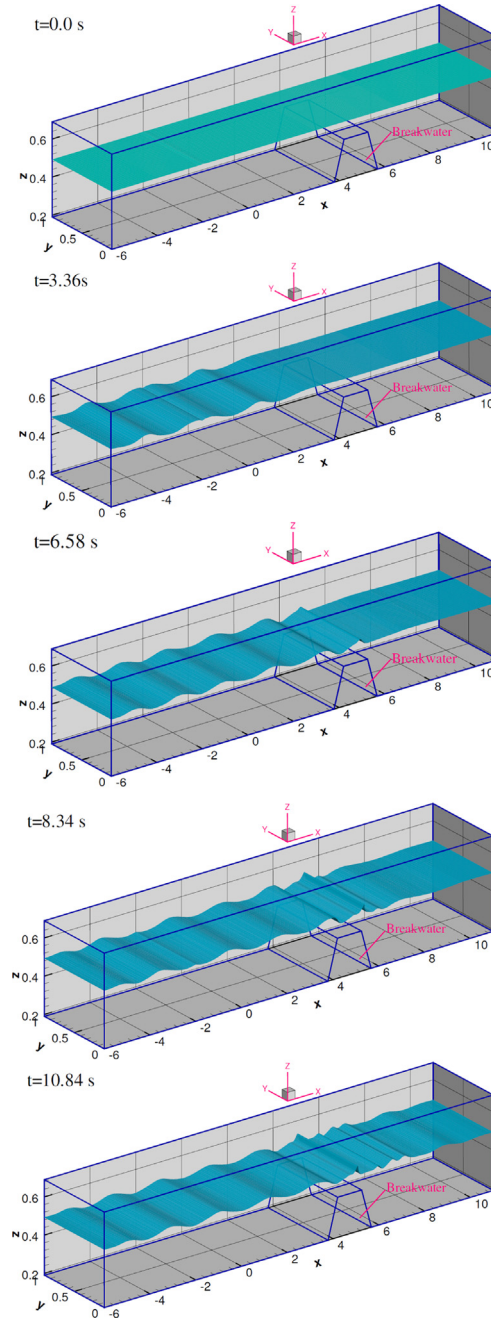


Fig. 10. 3-D wave profile at several typical times determined by the FSSI-CAS 3D in the process of wave, sand bed and breakwater interaction.

$d_{50}$  could not be sufficiently described by Darcy's law (only based on laminar flow). The turbulent flow induced nonlinear drag force is also very significant for the porous flow in rubble mound breakwater. In order to more accurately simulate the interaction between the wave and porous medium with huge  $d_{50}$ , it is necessary to develop a new 3-D wave model to consider the turbulent flow induced nonlinear drag force, the inertial effect and the viscous effect for porous flow in the future, where the interaction between the porous flow and solid matrix could be formulated as (Hur et al., 2008).

$$f_{Di} = C_D \frac{\mu}{d_{50}^2} \frac{(1-n)^2}{n} u_{fi} + F_D \frac{(1-n)}{d_{50}} u_{fi} \sqrt{|u_{fj} u_{fj}|}, \tag{12}$$

where  $F_D$  is the turbulent porous flow induced drag force coefficient.

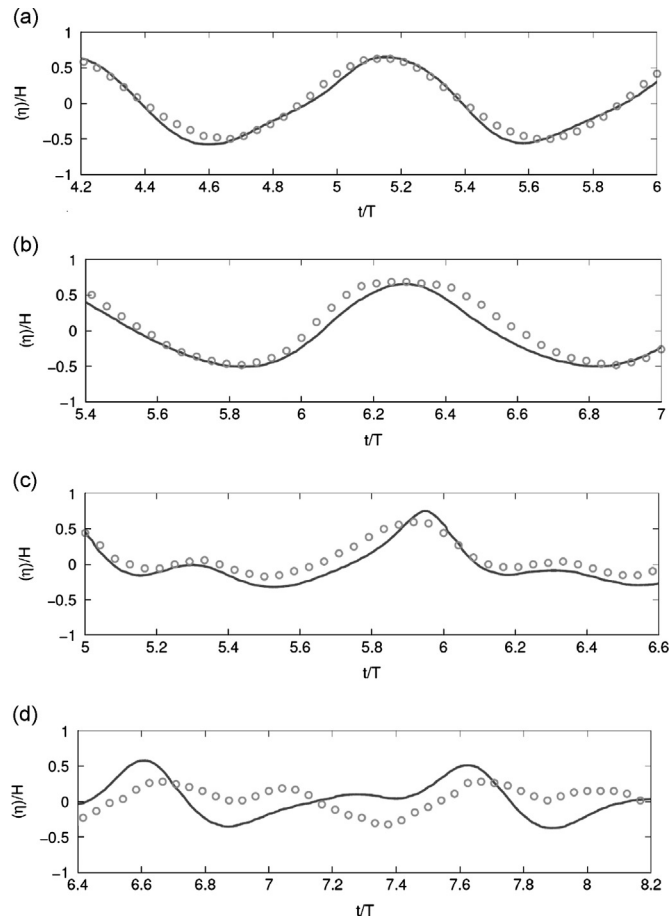


Fig. 11. Comparison of the wave profile at four typical positions *a*, *b*, *c* and *d*. Solid line: numerical results, circles: experimental results.

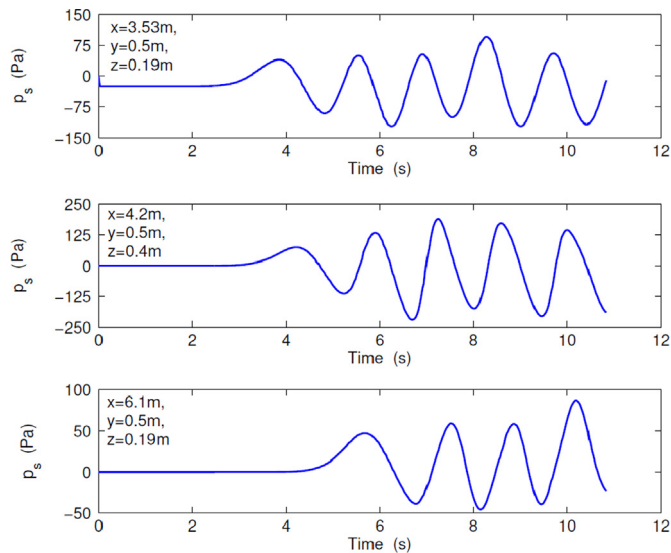


Fig. 12. Wave-induced dynamic pressure acting on sand bed and breakwater.

### 3.2.3. Dynamic response

Under the 3-D wave loading, the sand bed and breakwater respond accordingly to it. When the 3-D wave propagates on the sand bed and breakwater, the wave-induced pressure is applied to the surface of sand bed and breakwater through the

developed data exchange port. Taking the wave-induced pressure acting on the sand bed and breakwater as the boundary condition, the dynamic response of the sand bed and breakwater is determined by the soil model.

Fig. 12 illustrates the 3-D wave-induced pressure acting on the sand bed and breakwater. Three typical positions are chosen: the point on sand bed in front of breakwater ( $x=3.53$  m,  $y=0.5$  m,  $z=0.19$  m), the point on the breakwater ( $x=4.2$  m,  $y=0.5$  m,  $z=0.4$  m), and the point behind the breakwater ( $x=6.1$  m,  $y=0.5$  m,  $z=0.19$  m). From Fig. 12, it is found that the wave induced pressure on sand bed and breakwater are all periodic, and the pressure acting on the breakwater is most significant. Before the 3-D wave arrives at the sand bed or breakwater, the wave induced pressures are all zero.

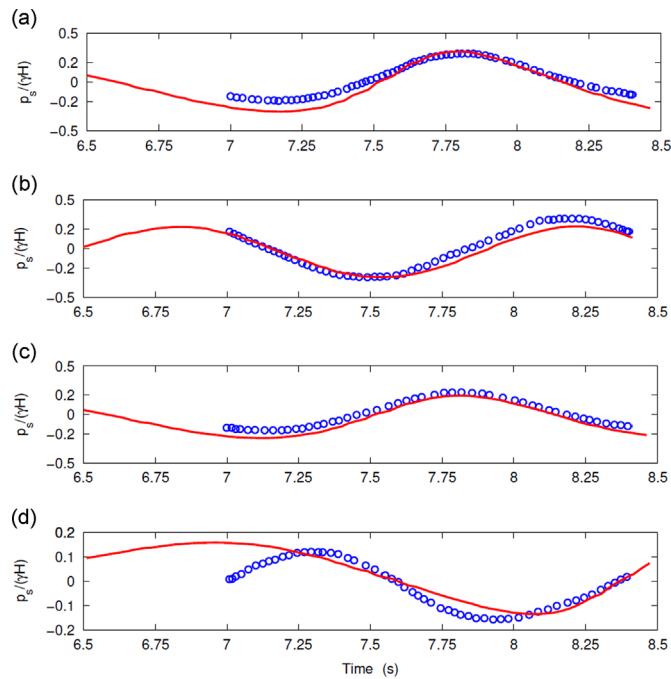


Fig. 13. Comparison of the wave-induced pore pressure at four typical positions A, B, C and D. Solid line: numerical results, circles: experimental results.

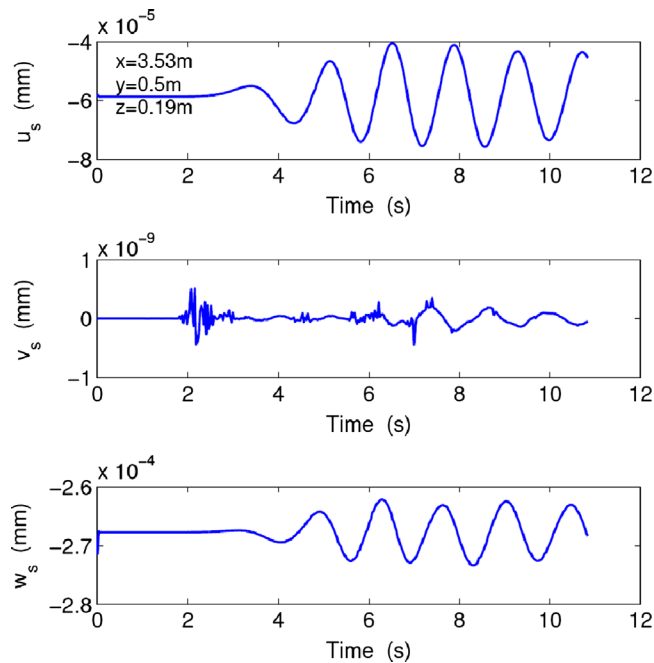


Fig. 14. Wave-induced displacements on sand bed at ( $x=3.53$  m,  $y=0.5$  m,  $z=0.19$  m) which is in front of breakwater.

Fig. 13 demonstrates the comparison of the wave induced pore pressure at four typical positions A, B, C and D in the sand bed between the experimental data and the numerical results. As demonstrated in Fig. 13, the agreement between the numerical results determined by FSSI-CAS 3D and the experimental data (Mizutani et al., 1998) is good. However, there is also a phase difference between the numerical results and the experimental data (Mizutani et al., 1998) at point D. As analyzed in Section 3.2.2 (3-D wave field), this phase difference would also be attributed to the inappropriate usage of a simple formulation (Eq. (10)) to describe the drag force between the porous flow and the solid matrixes in the breakwater.

The comparison of the wave profile at positions *a*, *b*, *c* and *d*, and the comparison of wave induced pore pressure in sand bed and breakwater at positions A, B, C and D indicate that the developed 3-D coupled model for the fluid–structure–seabed interaction is highly reliable.

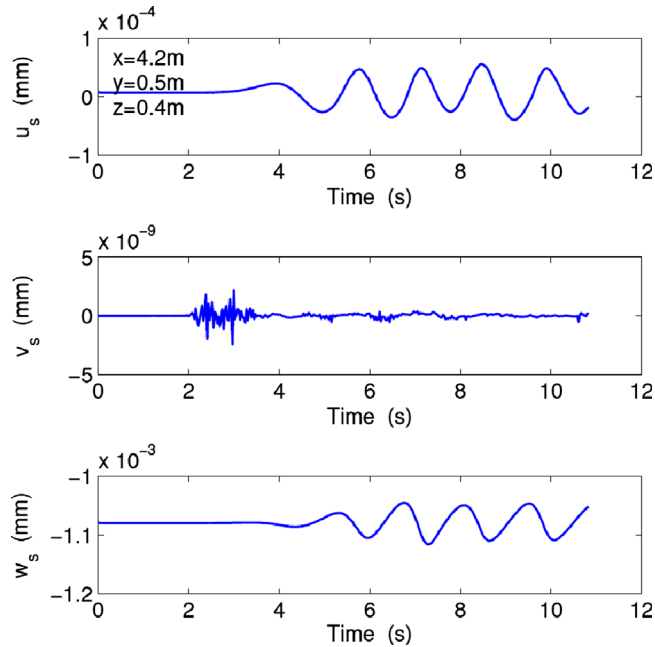


Fig. 15. Wave-induced displacements at ( $x=4.2$  m,  $y=0.5$  m,  $z=0.4$  m) which is on breakwater.

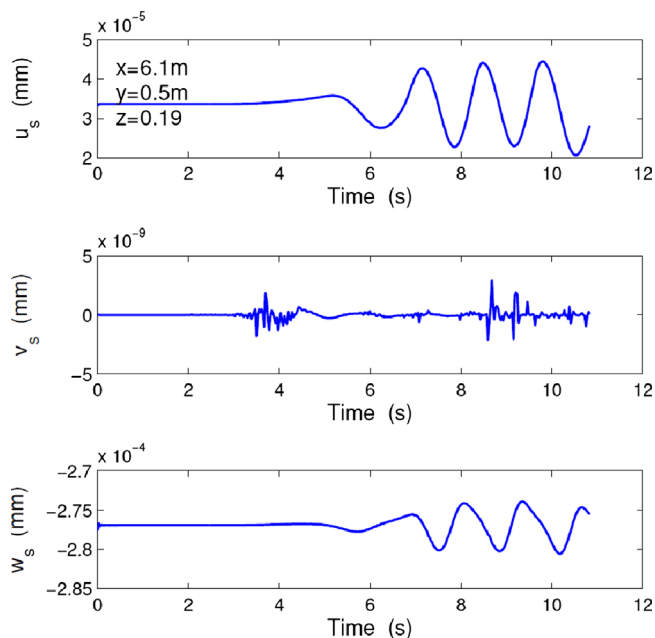


Fig. 16. Wave-induced displacements on sand bed at ( $x=6.1$  m,  $y=0.5$  m,  $z=0.19$  m) which is behind breakwater.

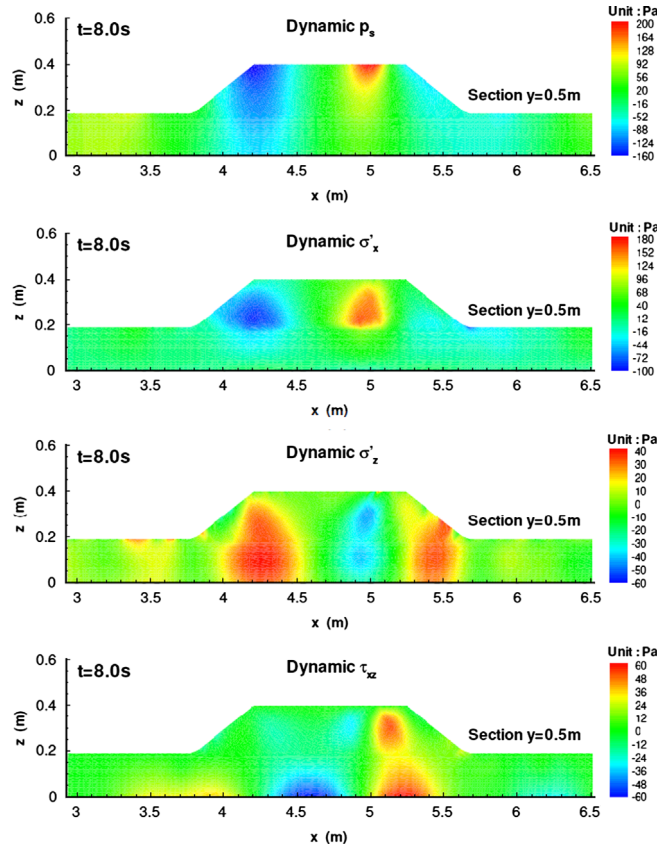


Fig. 17. Wave-induced dynamic pore pressure and effective stresses in sand bed and breakwater at time  $t=8.0$  s.

Figs. 14–16 show the wave induced displacements of the sand bed and breakwater on the three typical positions which coincide with the three positions in Fig. 12. From Figs. 14–16, it is found that the sand bed and breakwater vibrate periodically under the 3-D wave loading. The wave-induced displacement in  $y$  direction  $v_s$  is apparently small ( $O(10^{-9})m$ ) relative to the displacements in the other two directions. The vertical displacement  $w_s$  is one order of magnitude greater than the horizontal displacement  $u_s$  for both sand bed and breakwater at all the three points. Another phenomenon observed from Figs. 14–16 is that the horizontal and vertical displacements  $u_s$  and  $w_s$  of the breakwater are both one order of magnitude greater than the counterparts of the sand bed. It is indicated that the dynamic response of breakwater to the 3-D wave is much stronger than that of sand bed.

Fig. 17 illustrates the distribution of the wave-induced dynamic response in the sand bed and breakwater at time  $t=8.0$  s (the section  $y=0.5$  m is chosen). It is found that the wave-induced pore pressure is negative under the wave trough, while it is positive under wave crest. The wave induced pore pressure in the range of  $x=5.2-6.0$  m in the sand bed and breakwater is mainly  $-60$  Pa to  $-80$  Pa, which is much less than that in the range of  $x=4.0-4.5$  m (both areas are under wave trough). It is indicated that the rubble mound breakwater indeed could effectively dissipate the wave energy when the 3-D wave is passing through it.

In Fig. 17, it can also be observed that  $\sigma'_x$  is compressive, and  $\sigma'_z$  is tensile under wave trough; oppositely,  $\sigma'_x$  is tensile, and  $\sigma'_z$  is compressive under wave crest. This is because of the fact that the wave trough pulls the sand bed and breakwater under it, while the wave crest compresses the sand bed and breakwater under it. The wave-induced shear stress mainly concentrates in the lower part of sand bed under the breakwater.

#### 4. Conclusion

In this study, a 3-D coupled numerical model for the fluid–structures–seabed interaction is developed, in which two sub-models (soil model and wave model) are included. Biot's dynamic equation (' $u-p$ ' approximation) is taken as the governing equation in soil model, and solved using the finite element method. The modified Navier–Stokes equation, in which the drag force involved in porous flow is considered, is taken as the governing equation in wave model, and solved using the finite volume method. The two sub-models are coupled together through a non-matched mesh scheme and non-match time step scheme. A data exchange port based on the shepherd interpolation method is developed to transmit the data at the interface between the fluid domain and the seabed/breakwater domain. This developed 3-D coupled model is validated by an

analytical solution, and a laboratory wave flume test conducted by Mizutani et al. (1998). The good agreement between the numerical results determined by FSSI-CAS 3D for the wave profile and wave-induced pore pressure in the sand bed and breakwater indicates that the 3-D coupled numerical model FSSI-CAS 3D is reliable.

## Acknowledgments

The authors Prof. Wang and Prof. Zhu thank the financial support from Chinese 973 Project: Evolutionary Trends and Sustainable Utilization of Coral Reefs in the South China Sea (2013CB956104). The author Ye Jianhong and Jeng Dongsheng are grateful for the financial support from EPSRC#EP/G006482/1. The author Ye Jianhong also appreciates the funding support of Overseas Research Student Award from Scottish Government, UK.

## References

- Carman, P.C., 1937. Fluid flow through granular beds. *Transactions of the Institution of Chemical Engineers* 15, 150–166.
- Chan, A.H.C., 1988. A Unified Finite Element Solution to Static and Dynamic Problems of Geomechanics (Ph.D. Thesis). University of Wales, Swansea Wales.
- Cheng, Y.Z., Wang, Y.X., Jiang, C.B., 2007. Coupling model of nonlinear wave and sandy seabed dynamic interaction. *China Ocean Engineering* 21, 77–89.
- Chung, S.G., Kim, S.K., Kang, Y.J., Im, J.C., Prasad, K.N., 2006. Failure of a breakwater founded on a thick normally consolidated clay layer. *Geotechnique* 56, 393–409.
- Franco, L., 1994. Vertical breakwaters: the Italian experience. *Coastal Engineering* 22, 31–55.
- Hsu, J.R.C., Jeng, D.S., 1994. Wave-induced soil response in an unsaturated anisotropic seabed of finite thickness. *International Journal for Numerical and Analytical Methods in Geomechanics* 18, 785–807.
- Hsu, J.R.C., Jeng, D.S., Tsai, C., 1993. Short-crested wave-induced soil response in a porous seabed of infinite thickness. *International Journal for Numerical and Analytical Methods in Geomechanics* 17, 553–576.
- Hur, D.S., Kim, C.H., Kim, D.S., Yoon, J.S., 2008. Simulation of the nonlinear dynamic interactions between waves, a submerged breakwater and the seabed. *Ocean Engineering* 35, 511–522.
- Hur, D.S., Kim, C.H., Yoon, J.S., 2010. Numerical study on the interaction among a nonlinear wave, composite breakwater and sandy seabed. *Coastal Engineering* 57, 917–930.
- Hur, D.S., Mizutani, N., 2003. Numerical estimation of the wave forces acting on a three-dimensional body on a submerged breakwater. *Coastal Engineering* 47, 329–345.
- Lin, Z.P., Liu, P.L.-F., 1999. Internal wave-maker for Navier–Stokes equations models. *Journal of Waterway, Port, Coastal, and Ocean Engineering* 99, 207–215.
- Los Alamos National Laboratory (LANL), May 2009. TRUCHAS Physics and Algorithms-Version 2.5.3.
- Lundgren, H., Lindhardt, J.H.C., Romold, C.J., 1989. Stability of breakwaters on porous foundation. In: *Proceeding of the 12th International Conference on Soil Mechanics and Foundation Engineering*, vol. 1. pp. 451–454.
- Mase, H., Sakai, T., Sakamoto, M., 1994. Wave-induced pore water pressure and effective stresses around breakwater. *Ocean Engineering* 21, 361–379.
- Mizutani, N., Mostafa, A.M., 1998. Dynamic interaction of nonlinear waves and a seawall over sand seabed. *International Journal of Offshore and Polar Engineering* 8, 30–38.
- Mizutani, N., Mostarfa, A., Iwata, K., 1998. Nonlinear regular wave, submerged breakwater and seabed dynamic interaction. *Coastal Engineering* 33, 177–202.
- Mizutani, N., Mostafa, A.M., Iwata, K., 1999. Numerical modeling of nonlinear interaction between wave and composite breakwater over sand bed. *Journal of Hydraulic Coastal and Environmental Engineering JSCE* 614, 121–133.
- Mostafa, A., Mizutani, N., Iwata, K., 1999. Nonlinear wave, composite breakwater and seabed dynamic interaction. *Journal of Waterway, Port, Coastal, and Ocean Engineering* 25, 88–97.
- Ou, J.H., 2009. Three-Dimension Numerical Modeling of Interaction Between Soil and Pore Fluid (Ph.D. Thesis). University of Birmingham, Birmingham UK.
- Tsai, C.P., 1995. Wave-induced liquefaction potential in a porous seabed in front of a breakwater. *Ocean Engineering* 22, 1–18.
- Tsai, C.P., Lee, T.L., Hsu, J., 2000. Effects of wave nonlinearity on the standing wave-induced seabed response. *International Journal for Numerical and Analytical Methods in Geomechanics* 24, 869–892.
- Ulker, M.B.C., Rahman, M.S., Guddati, M.N., 2010. Wave-induced dynamic response and instability of seabed around caisson breakwater. *Ocean Engineering* 37, 1522–1545.
- Ulker, M.B.C., Rahman, M.S., Guddati, M.N., 2012. Breaking wave-induced response and instability of seabed around caisson breakwater. *International Journal for Numerical and Analytical Methods in Geomechanics* 36, 362–390.
- Ye, J.H., Jeng D.S., Liu P.L.-F., Chan A.H.C. Breaking wave-induced response of composite breakwater and liquefaction of seabed. *Coastal Engineering*, submitted for publication.
- Ye, J.H., Jeng, D.S., Wang, R., Zhu, C.Q. A 2-D semi-coupled numerical model for fluid–structures–seabed interaction: model and validation. *Journal of Fluids and Structures*, <http://dx.doi.org/10.1016/j.jfluidstructs.2013.04.008>, in press.
- Ye, J.H., 2012. Numerical Analysis of Wave–Seabed–Breakwater Interaction (Ph.D. Thesis), University of Dundee, Dundee, United Kingdom.
- Zienkiewicz, O.C., Chang, C.T., Bettess, P., 1980. Drained, undrained, consolidating and dynamic behaviour assumptions in soils. *Geotechnique* 30, 385–395.